AGU
ADVANCING
EARTH AND
SPACE SCIENCES

Geophysical Research Letters®

Key Points:

- The first report of K-H waves and magnetic reconnection occurring simultaneously at the magnetopause LLBL under southward IMF conditions
- The reconnection ion jets are observed at both the leading and trailing edges of the K-H waves
- Favorable conditions for reconnection are produced by K-H waves and reconnection may in turn affect the global evolution of the K-H waves

Correspondence to:

W. Li and C. Wang,
wyli@spaceweather.ac.cn;
cw@spaceweather.ac.cn

Kelvin-Helmholtz Waves and Magnetic Reconnection at the Earth's Magnetopause Under Southward Interplanetary Magnetic Field

Tongkuai Li[1,2], Wenya Li[1,3], Binbin Tang[1], Yuri. V. Khotyaintsev[4], Daniel Bruce Graham[4], Akhtar Ardakani[5], J. L. Burch[6], D. J. Gershman[7,8], B. Lavraud[9,10], C. T. Russell[11], Quanming Lu[3], Xiaocheng Guo[1,2], and Chi Wang[1,2]

[1]State Key Laboratory of Space Weather, National Space Science Center, Chinese Academy of Sciences, Beijing, P. R. China, [2]College of Earth and Planetary Sciences, University of Chinese Academy of Sciences, Beijing, P. R. China, [3]Key Laboratory of Geospace Environment, University of Science and Technology of China, Hefei, P. R. China, [4]Swedish Institute of Space Physics, Uppsala, Sweden, [5]Institute for the Study of Earth, Oceans, and Space, University of New Hampshire, Durham, NH, USA, [6]Southwest Research Institute, San Antonio, TX, USA, [7]NASA Goddard Space Flight Center, Greenbelt, MD, USA, [8]Department of Astronomy, University of Maryland, College Park, MD, USA, [9]Laboratoire d'Astrophysique de Bordeaux, University Bordeaux, CNRS, Pessac, France, [10]Institut de Recherche en Astrophysique et Planétologie, Université de Toulouse, CNRS, UPS, CNES, Toulouse, France, [11]Department of Earth and Space Sciences, University of California, Los Angeles, Los Angeles, CA, USA

Abstract We present Magnetospheric Multiscale (MMS) observations of a K-H wave event under southward IMF conditions, accompanied by ongoing magnetic reconnection. The nonlinear K-H waves are characterized by quasi-periodic fluctuations, the presence of low-density and high-speed ions, and variations in the boundary normal vectors at both the leading and trailing edges. Our observations reveal clear evidence of on-going magnetic reconnection through the identification of Alfvénic ion jets and the escape of energetic magnetospheric electrons. Among the 36 magnetopause current-sheet crossings in this event, 19 exhibit unambiguous signatures of reconnection at both the leading (7) and trailing (12) edges. Notably, the estimated current-sheet thicknesses at both edges are comparable to the ion-inertial scale, confirming the compression effect resulting from the large-scale evolution of the K-H waves. The reconnection jets potentially contribute to the suppression of K-H growth through boundary-layer broadening and the development of complex flow and magnetic field patterns.

Plain Language Summary Kelvin-Helmholtz (K-H) waves and magnetic reconnection are two common occurrences at the Earth's magnetopause, playing crucial roles in the transfer of mass, momentum, and energy from the solar wind to the magnetosphere. While extensive research has been conducted on the relationship between K-H waves and magnetic reconnection under northward interplanetary magnetic field (IMF) conditions, there is a notable gap in our understanding regarding the southward IMF scenario. This study presents the first observed event of K-H waves under southward IMF conditions, accompanied by magnetic reconnection, and provides a detailed analysis of the characteristics of both phenomena. Through our observations, we investigate the correlation between K-H waves and magnetic reconnection during southward IMF periods. Our findings suggest that the coexistence of K-H waves and magnetic reconnection may be attributed to the promoting effect of K-H waves on the occurrence of magnetic reconnection. Furthermore, it is likely that magnetic reconnection suppresses the evolution of K-H waves, which could potentially contribute to the low likelihood of observing K-H waves under southward IMF conditions.

1. Introduction

Kelvin-Helmholtz (K-H) instability can be triggered at the boundary of two plasma regions with sufficiently large velocity shear (Chandrasekhar, 1961; Miura & Pritchett, 1982; Pu & Kivelson, 1983a, 1983b). The low-latitude magnetopause boundary layer of the Earth's magnetosphere is characterized by a large velocity shear between the magnetosheath, with a large anti-sunward flow of shocked solar wind, and the nearly stagnant magnetosphere (Fairfield, 1971; Sckopke et al., 1981; Sonnerup, 1980). The excitation and evolution of the K-H instability along the magnetopause under various solar wind conditions have been analyzed extensively with in situ observations (Fairfield et al., 2000; Hasegawa et al., 2004; Lin et al., 2014; Lu et al., 2019; Taylor et al., 2012), local numerical

simulations (Ma et al., 2014a, 2014b; Nakamura et al., 2004; Nykyri & Otto, 2001), and global simulations (Claudepierre et al., 2008; Guo et al., 2010; Li et al., 2012, 2013). A number of studies suggest that K-H waves can cause effective transfer of solar wind mass, momentum, and energy across the magnetopause, especially under northward interplanetary magnetic field (IMF). Magnetic reconnection associated with the K-H waves is widely suggested to break the frozen-in condition of plasma at the magnetopause and produces significant mass and energy transport (Hasegawa et al., 2009; Nakamura et al., 2006; Nykyri & Otto, 2001; Nykyri et al., 2017).

When the IMF points northward, the K-H instability criterion can be easily satisfied at the low-latitude boundary layer (Chandrasekhar, 1961), and the K-H waves are frequently reported from the in situ observations (Hasegawa et al., 2006; Lin et al., 2014; Taylor et al., 2012). The well-developed K-H waves can increase the magnetic shear across the magnetopause, and the centrifugal force induced by the K-H waves can further compress the magnetopause current sheet down to ion inertial scale. This process predominantly occurs at the trailing or sunward edges of the K-H waves, where then the magnetic reconnection can be triggered (Hasegawa et al., 2009; Nakamura et al., 2013). Here, a trailing edge in in situ observations is represented by a magnetopause crossing from the magnetosphere to magnetosheath. With the advantage of high-resolution plasma and fields instruments, the Magnetospheric Multiscale (MMS) spacecraft recorded direct evidence of on-going magnetic reconnection induced by K-H waves under northward IMF on 8 September 2015, and this event was analyzed by tens of studies from different aspects (e.g., Eriksson et al., 2016; Li et al., 2016; Nakamura et al., 2017; Settino et al., 2021, 2022; Stawarz et al., 2016; Vernisse et al., 2016, 2020).

According to the linear theory from Chandrasekhar (1961), the K-H instability criterion is not affected by the signs of the magnetic fields on both sides of the boundary, and one would expect a similar probability of observing K-H waves under southward IMF conditions. However, there have been far fewer reports of K-H waves at the low-latitude magnetopause during southward IMF (Blasl et al., 2022; Hwang et al., 2011; Yan et al., 2014). Several numerical simulation studies suggest that magnetic reconnection at the magnetopause can suppress the generation and growth of Kelvin-Helmholtz waves under southward IMF (Nakamura et al., 2020, 2022; Wang et al., 2023). Ma et al. (2014a) demonstrated that the KHI is capable of inducing reconnection under southward IMF conditions in a three-dimensional (3D) framework. Nakamura et al. (2020) demonstrated that magnetic reconnection is triggered at multiple locations along the K-H wave edges in their early nonlinear stage based on a 3D fully kinetic simulation of K-H waves under southward IMF. The reconnection outflow ejects along the south-north direction, which is nearly perpendicular to both the shear flow and the K-H wave vector. The coupling between the complex flow and the magnetic field pattern in the boundary layer leads to a rapid decay of the K-H waves, and the process may reduce the observational probability of K-H waves under southward IMF. However, there has been no analysis of the interaction between K-H waves and magnetic reconnection under southward IMF using in situ data.

Blasl et al. (2022) reported an MMS event of the K-H waves under southward IMF. Combining the results from a two-dimensional (2D) simulation (Nakamura et al., 2022), they demonstrated that the lower-hybrid waves can cause a flattening of the magnetopause boundary layer, indicating the connection between the large and ion kinetic scales in the K-H waves. However, no clear signature of on-going magnetic reconnection was observed in that event. Nykyri et al. (2006) documented a K-H wave event associated with magnetic reconnection by Cluster when the varying IMF was predominantly Parker-spiral orientation and had a southward component for a short interval (~15 min). Kronberg et al. (2021) showed a Cluster event of Pc4 frequency K-H waves with reconnection at high-latitude magnetopause under southward IMF. In this Letter, we present an MMS event recorded on 26 June 2020, which shows observations of K-H waves and on-going magnetic reconnection at the magnetopause LLBL under southward IMF. The features of the tailward propagating K-H waves and the reconnection jets on both the leading and trailing edges of the K-H waves are analyzed in detail.

2. An Overview of the MMS Observations

This study examines the MMS observations on 26 June 2020 at the dawnside magnetopause. The MMS spacecraft were located at $(-15.8, -19.8, -1.0)$ Earth radii (R_E) in Geocentric Solar Ecliptic (GSE) coordinates. We use both the fast-mode (4.5 s resolution) and burst-mode (0.15 s for ions and 0.03 s for electrons) plasma data from the Fast Plasma Investigation (FPI, Pollock et al., 2016). We use magnetic field data from the Fluxgate Magnetometer (FGM, Russell et al., 2016) and electric field data from the Electric Double Probes (EDP, Ergun et al., 2016; Lindqvist et al., 2016). We focus on the large-scale and ion-scale processes in the investigated
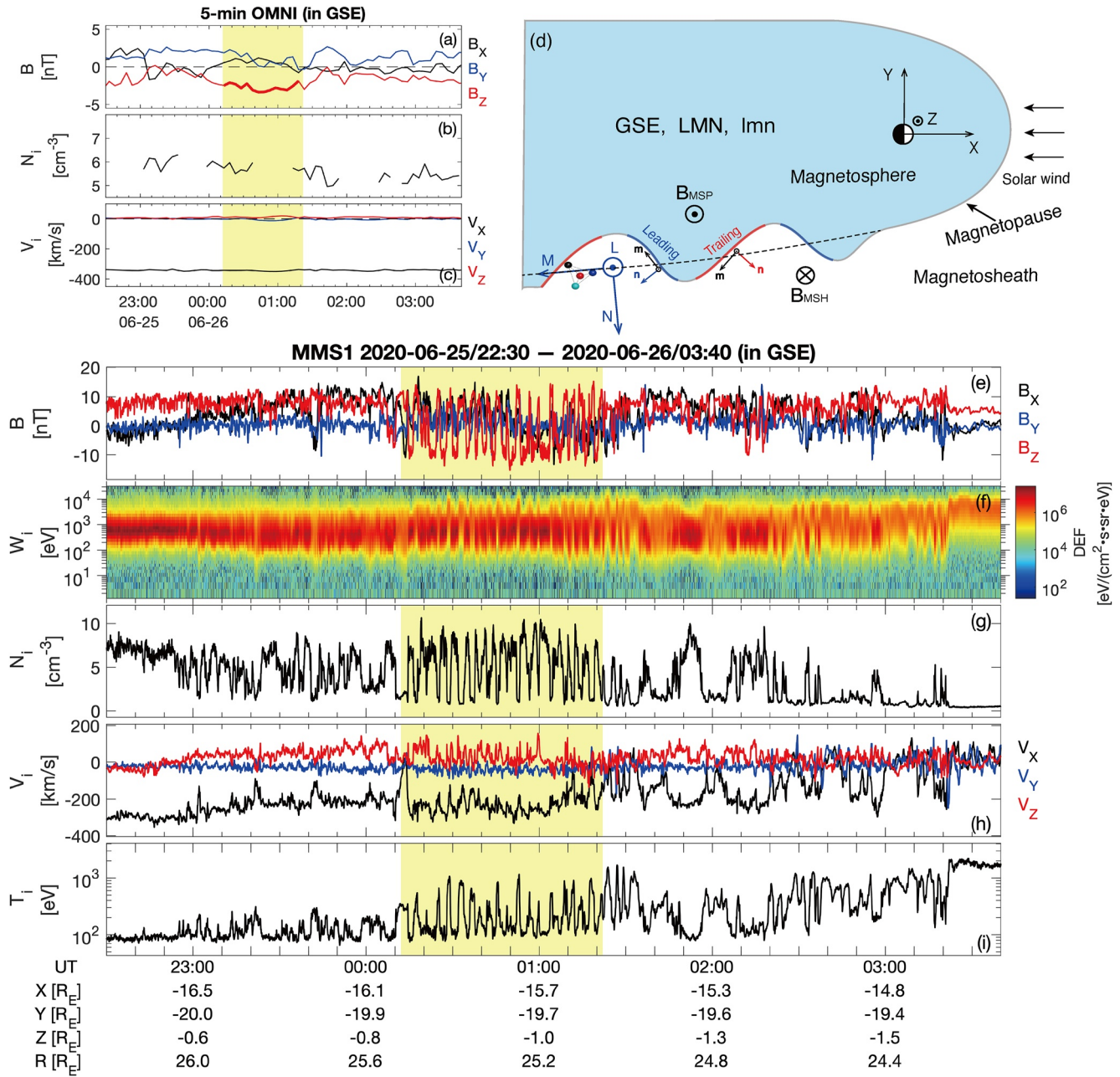
Figure 1. OMNI solar-wind data and MMS1 observations from 22:30 UT on 25 June to 03:40 UT on 26 June in 2020. 5-min OMNI data of (a) magnetic field **B**, (b) ion number density N_i, and (c) ion bulk velocity $\mathbf{V_i}$. The time is shifted by 13 min to show the real-time solar-wind conditions for MMS. (d) A schematic to show the MMS observations of the K-H waves at the dawnside magnetopause and the coordinate systems used in this study. MMS1 observations of (e) **B**, (f) ion omni-directional differential energy flux (energy spectrogram), (g) N_i, (h) $\mathbf{V_i}$, and (i) ion scaler temperature T_i. All vectors here are presented in Geocentric Solar Ecliptic (GSE) coordinates, and the MMS ion data are in fast mode. The yellow-shaded bars in (a)–(c) and (e)–(i) highlight the time interval when MMS encounter the Kelvin-Helmholtz waves during southward IMF.

interval. The four MMS spacecraft are separated by an average distance of 40 km, and their observations are almost identical. Thus, only results from MMS1 are presented in this study.

Figure 1 shows an observational overview of the dawnside magnetopause boundary layer by MMS1 and the OMNI solar-wind data between 22:30 UT on 25 June and 03:40 UT on 26 June in 2020. MMS are initially located in the magnetosheath, characterized by high density ($N_i \sim 6.9$ cm^{-3}, Figure 1g), fast tailward ion flow ($V_{iX} \sim -300$ km/s, Figure 1h), and low ion temperature ($T_i \sim 88$ eV, Figure 1i). From 22:55 UT on 25 June to 03:20 UT on 26

June, MMS observe a fluctuating magnetopause boundary layer, with variations in all physical parameters (Figures 1e–1i). After 03:20 UT on 26 June, MMS enter the magnetosphere, characterized by a dominant northward magnetic field ($B_Z \sim 5.4$ nT, Figure 1e), low density ($N_i \sim 0.4$ cm^{-3}), and nearly stagnant hot ions ($V_{iX} \sim 21$ km/s and $T_i \sim 1.8$ keV). In this study, we focus on the quasi-periodic perturbations from 00:12 UT to 01:22 UT on 26 June (as indicated by the yellow-shaded interval in Figures 1e–1i), with continuous burst-mode intervals.

In this time interval, a noticeable feature is that the B_Z component (red curve in Figure 1e) changes sign during the crossings between the magnetosphere and magnetosheath, indicating southward magnetic field in the solar wind. Figures 1a–1c show the 5-min OMNI solar-wind data, which have been time-shifted to enable direct comparison with the MMS observations. As shown in Figure 1a, the IMF is quasi-steady in the yellow-shaded interval, consistent with MMS observations in the magnetosheath. The IMF has an average value of (0.5, 0.9, −2.7) nT, dominated by a southward component. The solar-wind plasma conditions are also steady, with an average number density of 5.7 cm^{-3} and an average speed of 344 km/s. The bow-shock nose is estimated to be at (13.8, −1.2, −0.4) R_E based on the empirical model by Fairfield (1971). The time-shift of 13 min in Figure 1a–1c is estimated based on the straight-line distance between the bow-shock nose and MMS location, as well as a reduced solar-wind speed (300 km/s) to account for a slower shocked solar wind in the magnetosheath. Given the steady solar wind conditions and magnetopause boundary conditions, the perturbations shown in the yellow-shaded interval in Figures 1e–1i should be generated by local instability. The following section identifies these perturbations as surface waves generated by the K-H instability under southward IMF.

In this study, two sets of boundary-normal coordinate systems (see Figure 1d) are adopted for analyzing the K-H waves and the kinetic processes at each magnetopause crossing. The first one (LMN) is a large-scale (global) magnetopause boundary normal coordinate system. It is determined according to the empirical model by Shue et al. (1998), which yields **L** = (0.01, −0.04, 1.00), **M** = (−0.97, −0.25, 0.00), and **N** = (0.25, −0.97, −0.05). Here **L** is almost along Z-axis of GSE, and **M** is 14° away from -**X**. The other set (lmn) is the local current-sheet coordinate system. A preliminary local **n** is first determined by combining the results from the minimum variance analysis (MVA) and the timing analysis (Paschmann & Daly, 1998) on magnetic field data of each magnetopause current-sheet crossing. The local **l** is the maximum variance direction from MVA. The local **m** is the cross product of the preliminary local **n** and **l**, and the final **n** completes the right-hand orthogonal system. In the following sections, we will present a detailed analysis of the K-H waves observed in the LMN coordinate system, as well as the on-going magnetic reconnection observed in the lmn coordinate systems.

3. K-H Waves During Southward IMF

In order to identify the K-H waves within the time interval of the yellow-shaded bar in Figure 1, we adopt three criteria: (a) quasi-periodic fluctuations with periods between 1 and 5 min seen in the magnetic field and plasma parameters in the transition region between the magnetosheath and magnetosphere (Eriksson et al., 2016; Hasegawa et al., 2004, 2006; Li et al., 2016), (b) features of high-speed and low-density ions indicating the nonlinear stage of K-H vortices (Takagi et al., 2006), and (c) boundary normal vectors at the leading and trailing edges showing the K-H waveform.

Figure 2 presents a detailed overview of the quasi-periodic fluctuations observed at the magnetopause. From 00:14:35 UT to 01:20:35 UT, MMS recorded 18 sets of magnetosphere-magnetosheath (trailing edge) and magnetosheath-magnetosphere (leading edge) transitions, which correspond to 36 magnetopause current sheet crossings (vertical dashed lines in Figures 2a–2g). The period of the fluctuations is approximately 3.8 min (230 s), as estimated from the Fast Fourier Transform analysis on the magnetic field and number density data. These quasi-periodic fluctuations are observed in the magnetic field (Figure 2a), the ion energy spectrogram (Figure 2b), and the ion number density (Figure 2c). The fluctuations of the shear velocity (V_M, Figure 1d) is not prominent, suggesting fully developed K-H waves under nonlinear phase. Within the interval of Figure 2, the upstream solar-wind plasma conditions are steady (Figures 1b and 1c), and the IMF is quasi-steady and predominantly southward (Figure 1a). In this interval, no spacecraft can provide real-time magnetosheath conditions for MMS. We can only obtain them when MMS enter the magnetosheath. The magnetic field in the magnetosheath is approximately dominated by the B_L component (−10 nT, close to Z-axis of GSE). The ion number density of magnetosheath is about 8 cm^{-3}, and the V_M component is about 220 km/s, which can provide sufficient velocity shear to trigger the K-H instability (Chandrasekhar, 1961). MMS observe mirror modes in the magnetosheath, characterized by anti-correlation variations in the magnitude of magnetic field and ion number density, which are usually generated by ion temperature anisotropy downstream of a quasi-perpendicular shock (Balogh & Treumann, 2013; Vedenov & Sagdeev, 1961). Here, the period of the mirror
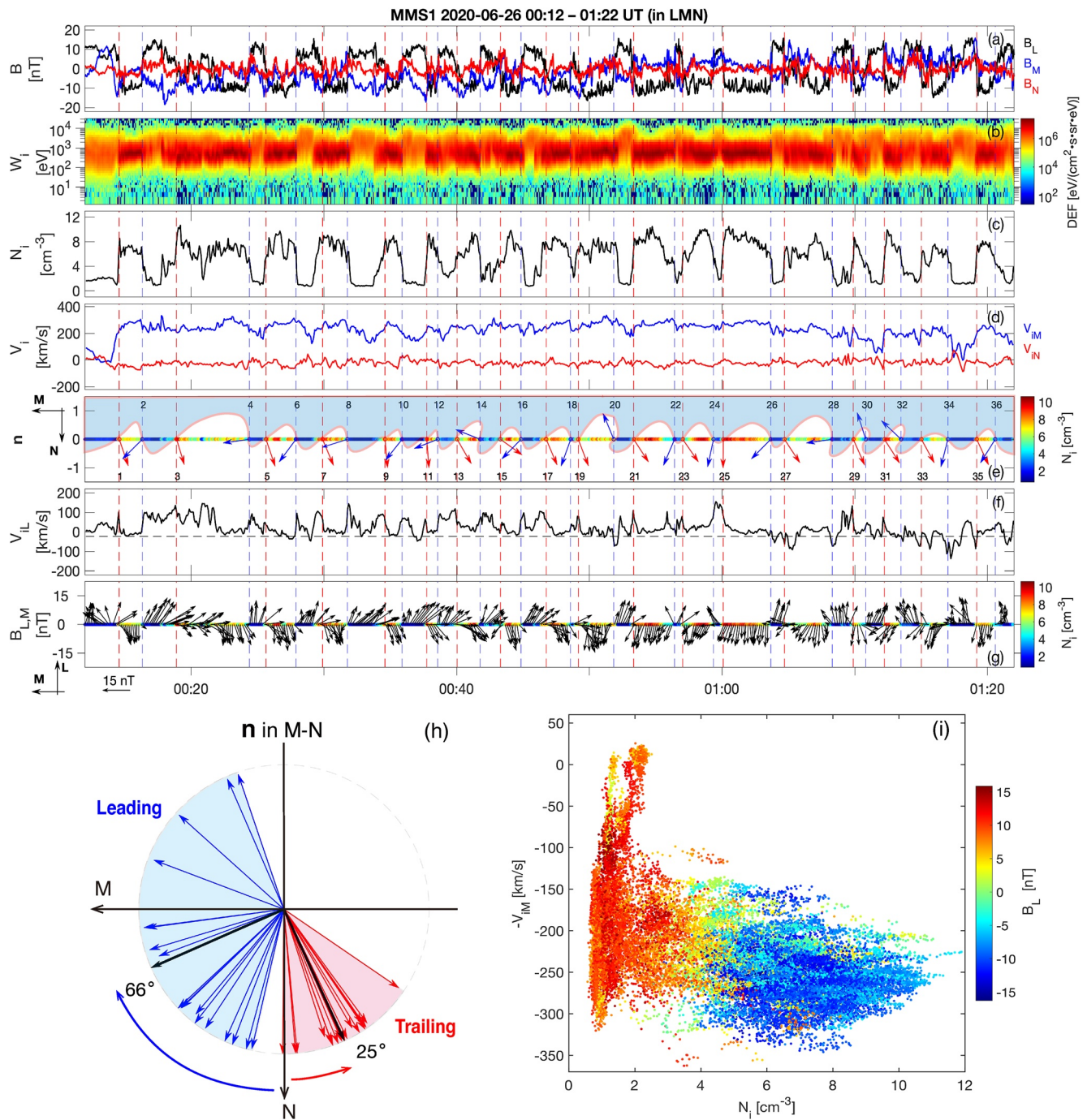
Figure 2. MMS1 observations of the K-H waves from 00:12 UT to 01:22 UT on 26 June 2020. (a) **B**. (b) Ion energy spectrogram. (c) N_i. (d) V_{iM} and V_{iN}. (e) 36 local boundary normal directions **n** in M-N plane, with a K-H wave sketch. The blue arrowed lines denote the leading edges, and the red ones denote the trailing edges. (f) V_{iL}. (g) **B** vectors projected in L-M plane to show the magnetopause current sheet crossings. The MMS trajectory in (e) and (g) is colored by N_i to show the quasi-periodic crossings between the magnetosheath and magnetosphere. (h) Normal vectors of 18 leading (blue) and 18 trailing (red) edges projected in M-N plane. The average deflection angles of **n** from N are 66° and 25° for the leading and trailing edges, respectively. (i) Scatter plot of N_i and $-V_{iM}$ in burst resolution to show the high-speed and low-density feature, with colors representing the B_L component.

modes is approximately 15 s and distinct from the period of the quasi-periodic magnetopause fluctuations, further implying that the long-period fluctuations are generated by local instability at the magnetopause.

Based on 3D magnetohydrodynamic (MHD) simulations of the K-H waves, Takagi et al. (2006) found that within highly rolled-up nonlinear K-H vortices, the tailward speed of the magnetospheric low-density plasma can reach

or even exceed that of the magnetosheath plasma. This so-called high-speed and low-density feature is widely observed in the non-linear K-H waves during northward IMF and has been observed in two cases during southward IMF (Blasl et al., 2022; Hwang et al., 2011). This high-speed and low-density feature is also prominent in our event, as shown by the left-bottom data points in Figure 2i. A K-H wave sketch is shown in Figure 2e, based on the local normal directions of the magnetopause current sheets (refer to Table S1 in Supporting Information S1). One can clearly see rolled-up structures, for example, the 14th and 20th current sheets. The nonlinear K-H waves during northward IMF usually have non-sinusoidal forms with steepened leading edges (Plaschke et al., 2016). In this reported case, the leading edges have tailward deflection angles between 13° and 161° relative to the large-scale **N** direction in the projected **M**-**N** plane, and the average deflection angle is 66°. The trailing edges have sunward deflection angles between −0.5° and 56°, with an average angle of 25° (Figure 2h). This indicates that the leading edges in this case are much steeper than the trailing edges, further suggesting the nonlinear stage of the observed K-H waves in Figure 2.

Based on the above features, the perturbations observed at the dawn magnetopause are identified as nonlinear K-H waves under southward IMF. The phase speed is estimated by the center-of-mass speed (244 km/s). Thus, the wavelength is about 8.8 R_E, which is comparable to that of the K-H waves at the same local time during northward IMF (Guo et al., 2010; Li et al., 2012; Lin et al., 2014). In the following section, we will demonstrate the on-going magnetic reconnection signatures at the K-H perturbed magnetopause.

4. On-Going Magnetic Reconnection at the K-H Boundary

The most remarkable feature of reconnection is the Alfvénic ion jet along the shear magnetic field direction. For the K-H waves shown in Figure 2, the magnetic field shear is predominantly along the **L** direction, and MMS observe several V_{iL} enhancements relative to the background flow, indicating the presence of ion jets resulting from on-going magnetic reconnection. We perform the Walén test to verify if the enhanced flow is consistent with a reconnection jet (Phan et al., 2004; Sonnerup, 1980). In this study, the Walén test is achieved by comparing the two vectors $\Delta \mathbf{V} = \mathbf{V}_j - \mathbf{V}_{MSH}$ and $\Delta \mathbf{V}_A = \mathbf{V}_{A,j} - \mathbf{V}_{A,MSH}$. Here, $\mathbf{V}_A = \mathbf{B}/\sqrt{\mu_0 \rho}$ is the Alfvén velocity, μ_0 is the permeability in vacuum, ρ is the plasma mass density, and "MSH" and "j" denote the magnetosheath and ion jet, respectively. The two vectors are evaluated along the **l** directions of all 36 magnetopause current sheets.

Figure 3 presents an example of a northward ion jet during a trailing edge crossing. The vectors are in lmn coordinates, where **l** = (0.90, −0.44, −0.12), **m** = (0.41, 0.68, 0.61), and **n** = (−0.20, −0.60, 0.78) in the global LMN coordinates. The blue-shaded and yellow-shaded intervals in Figures 3a and 3e highlight the magnetosheath reference region and the flow-enhanced region for the Walén test, respectively. ΔV_l is presented by the black curve in Figure 3e, and ΔV_{Al} is shown by the red one. The correlation coefficient (CC) between ΔV_l and ΔV_{Al} is 0.93, and the linear slope of $\Delta V_l / \Delta V_{Al}$ is 0.84. These illustrate a northward Alfvénic jet at the current sheet, and the jet peak speed locates on the magnetospheric side of the neutral line (green dashed line), consistent with the property of asymmetric reconnection at the magnetopause (Cassak & Shay, 2007).

Furthermore, we use the pitch-angle distribution properties of magnetosphere energetic electrons to verify the on-going reconnection. In this event, the typical energies of the magnetosheath electrons are tens of eV. The magnetosphere typically encompasses keV energetic electrons, and the analysis of their pitch-angle distributions can provide insights into the topology of the magnetospheric magnetic field lines, indicating whether they are close or open. One can expect anti-parallel and parallel moving energetic electrons in the northward ($V_{il} > 0$) and southward ($V_{il} < 0$) ion jets, respectively (Figure 3i). As shown in Figure 3g, MMS1 observes nearly isotropic energetic (1.5 − 25 keV) electrons inside the magnetopause (before the red dashed line) and dominant anti-parallel energetic electrons during the boundary layer crossing until the time indicated by the blue dashed line. After that, MMS enter magnetosheath, characterized by low electron temperature (Figure 3f) and negligible energetic electron population (Figures 3f and 3g). The observed pitch-angle distribution of the energetic electrons is consistent with a northward ion jet crossing (Figure 3i). Besides, MMS observe unambiguous Hall electric field with a magnitude of ∼2 mV/m at the magnetospheric separatrix.

We perform the same analysis on all 36 current sheets of the K-H waves, and 19 of them show unambiguous on-going reconnection features, with the Walén test slopes larger than 0.6, CC larger than 0.85, and consistent pitch-angle distributions of energetic electrons. The ion jets are found at both the leading and trailing edges of the K-H waves. MMS observe 7 (5 northward and 2 southward) reconnection jets at the leading edges and 12
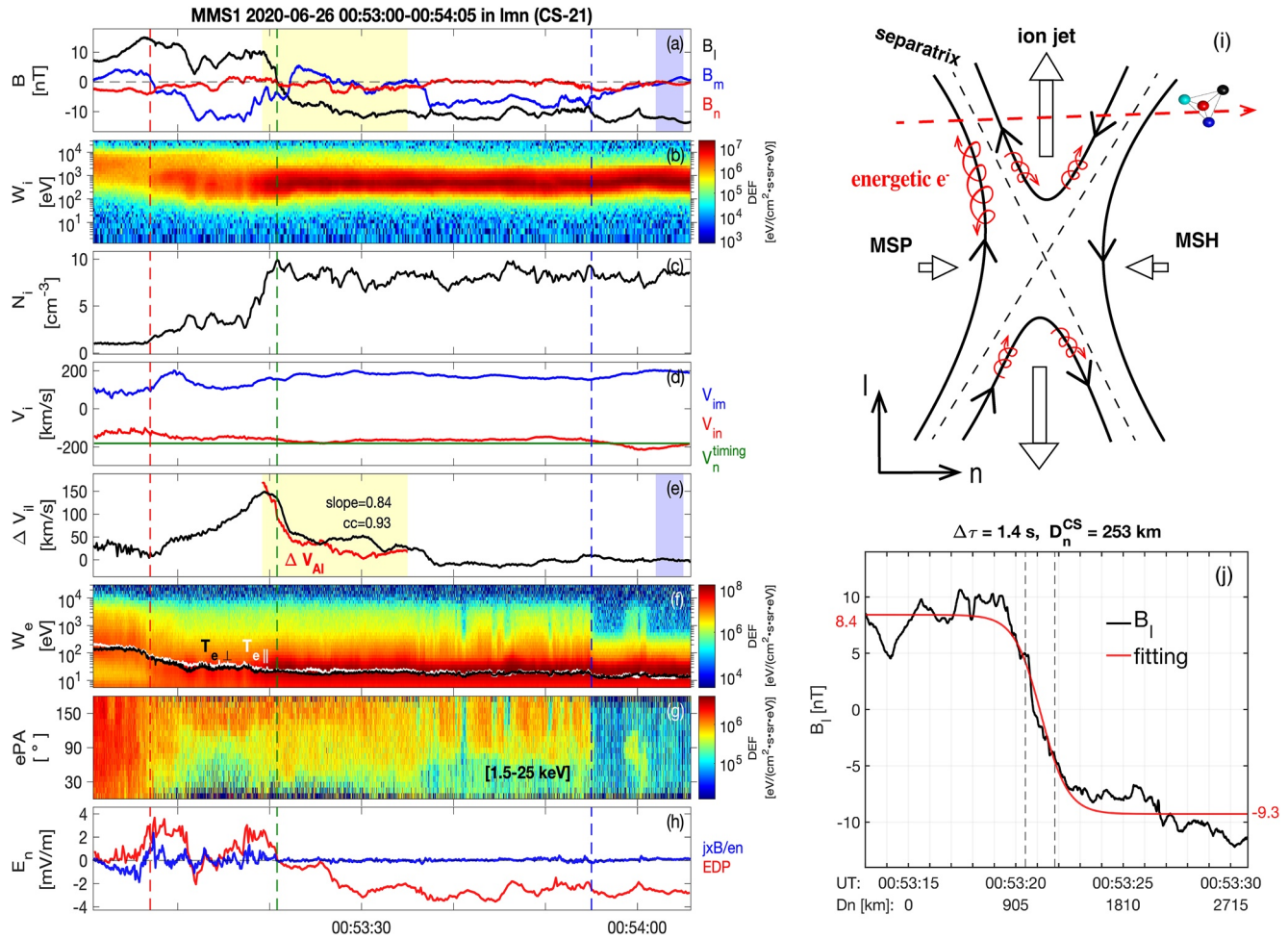
Figure 3. A northward reconnection jet observed at the 21st current sheet (trailing edge) in burst mode. (a) **B**. (b) Ion energy spectrogram. (c) N_i. (d) V_{im} and V_{in}, with the normal velocity V_n^{timing} from the timing analysis on magnetic field data. (e) Observed ΔV_{il} (black) and predicted one (red) based on the Walén relation. (f) Electron energy spectrogram with electron parallel ($T_{e\parallel}$) and perpendicular ($T_{e\perp}$) temperatures. (g) Pitch-angle distribution of magnetospheric energetic (1.5–25 keV) electrons. (h) **n** components of the observed E and Hall E term. The vertical green dashed line in (a)–(h) denotes the neutral line ($B_l = 0$) crossing. The red and blue dashed lines denote the magnetospheric and magnetosheath separatrixes. (i) A schematic of magnetic reconnection at the K-H active magnetopause, with a red dashed arrowed line representing the MMS crossing through a northward ion jet. (j) Estimation of the current-sheet thickness D_n^{CS} according to a Harris-type model fitting.

(10 northward and 2 southward) jets at the trailing edges, as shown in Figure 4a and listed in Table S1 of the Supporting Information S1.

Southward IMF conditions result in a large magnetic field shear at the low-latitude magnetopause, with magnetic reconnection frequently occurring at the dayside magnetopause. In the flank and nightside magnetopause regions, the current sheet is typically much thicker (Haaland et al., 2020) than the ion inertial length, thereby inhibiting magnetic reconnection in those regions. However, when K-H waves are generated due to the presence of strong velocity shear along the low-latitude boundary, the centrifugal force induced by these waves has the potential to compress the local current sheet down to the ion inertial scale (Eriksson et al., 2016; Li et al., 2016; Nakamura et al., 2006). To demonstrate the current-sheet thinning by the compression, we estimate the thicknesses of all the 36 magnetopause current sheet crossings. For the example shown in Figure 3, The green line in Figure 3d shows the boundary normal velocity V_n^{timing} calculated by the timing analysis on the four-spacecraft magnetic field data (Paschmann & Daly, 1998), which is comparable to the **n** component of $\mathbf{V_i}$. The B_l profile along time and the normal distance D_n is displayed by the black curve in Figure 3j. Here, D_n is computed from V_n^{timing} (181 km/s). To estimate the current-sheet thickness, we utilize the following Harris-type model to fit the B_l profile:
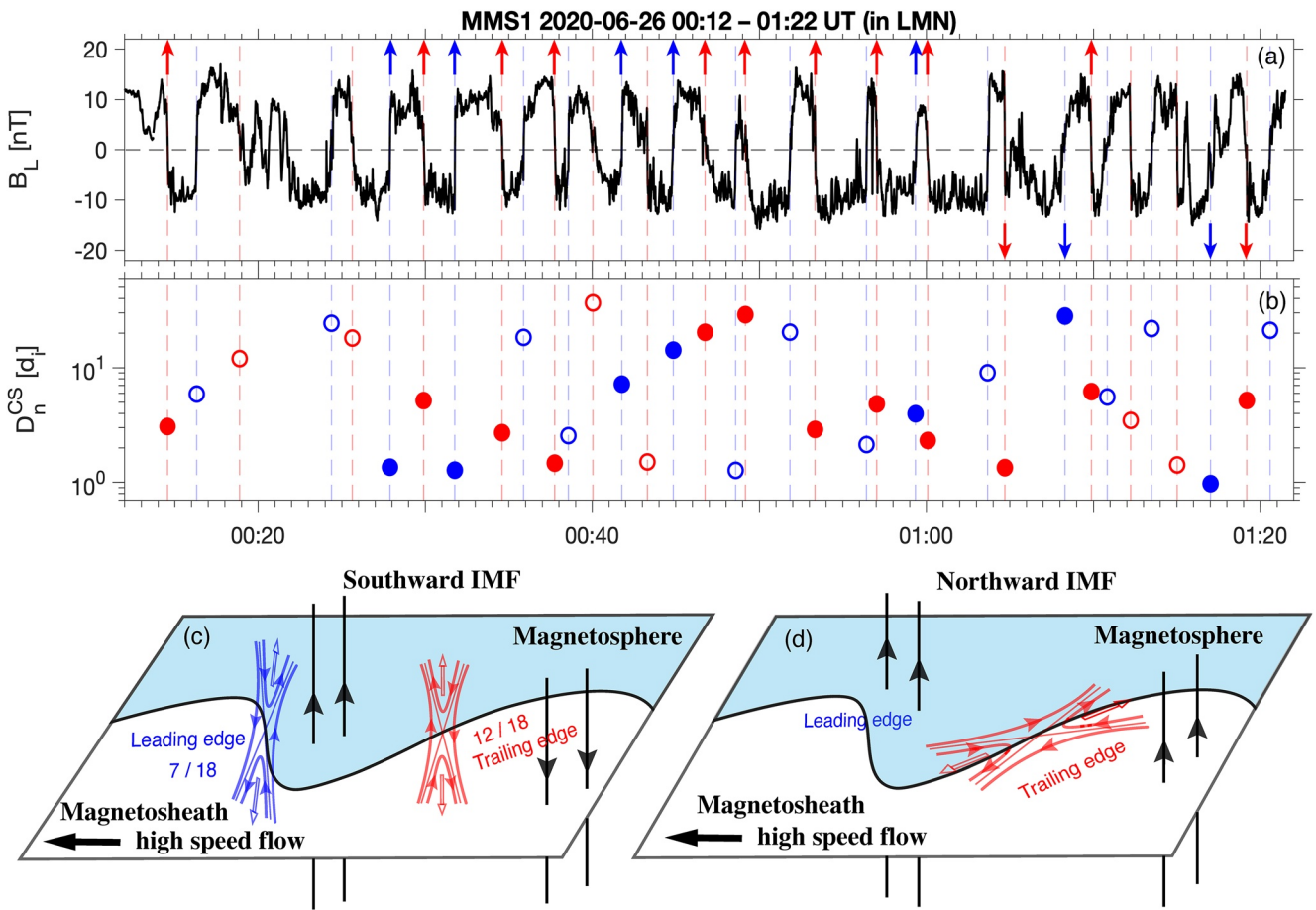
Figure 4. (a) B_L with arrows denoting the identified reconnection jets. The upward and downward arrows mean the northward and southward jets, respectively. (b) Current-sheet thickness D_n^{CS} of the 18 trailing (red) and 18 leading (blue) edges, with filled circles showing the current sheets with ion jets. Sketches showing (c) reconnection jets observed at the leading and trailing edges under southward IMF in this event and (d) reconnection jets only observed at the trailing edges under northward IMF. The black arrowed lines show the directions of magnetic field Bz components in the magnetosphere and magnetosheath.

$$B_l = \frac{B_{l1} e^{k\left(D_n - D_{n_0}\right)} + B_{l2} e^{-k\left(D_n - D_{n_0}\right)}}{e^{k\left(D_n - D_{n_0}\right)} + e^{-k\left(D_n - D_{n_0}\right)}}, \tag{1}$$

where B_{l1} and B_{l2} denote the magnetic field on either side of the current sheet, and k and D_{n_0} are the fitting parameters. In Figure 3j, $B_{l1} = -9.3$ nT and $B_{l2} = 8.4$ nT. We estimate the current-sheet thickness from the distance between $B_{l1}/2$ and $B_{l2}/2$, indicated by the two dashed lines in Figure 3j. The current-sheet thickness D_n^{CS} of the event in Figure 3 is 253 km, which is 2.9 d_i (d_i: 86 km, ion inertial length of the magnetosheath). Figure 4b shows the thicknesses of all the current sheets in our reported K-H wave event. The median D_n^{CS} of the leading edges is 563 km (6.5 d_i), and that of the trailing edges is 357 km (4.2 d_i).

5. Conclusion and Discussion

In this study, we present MMS observations of K-H waves accompanied by on-going magnetic reconnection at the dawnside magnetopause under southward IMF conditions. The K-H waves are identified by quasi-periodic fluctuations in plasma parameters and magnetic fields, along with distinct features of high-speed and low-density plasma. During the observation of K-H waves, the solar wind remains relatively stable, and the IMF is predominantly southward ([0.5, 0.9, −2.7] nT in GSE). The reported K-H waves have an estimated period of 3.8 min (230 s) and a wavelength of approximately 8.8 R_E. The K-H waveforms are sketched based on the local boundary

normal directions of the 36 magnetopause current-sheet crossings, displaying rolled-up vortex structures with steeper leading edges than trailing edges.

Among the 36 current-sheet crossings, 19 exhibit clear indications of on-going magnetic reconnection, including Alfvénic ion flows that satisfy the Walén relation and open magnetic field lines characterized by the escape of energetic magnetospheric electrons. Specifically, there are 7 reconnection jets (2 southward and 5 northward) observed at the leading edges, and 12 jets (2 southward and 10 northward) detected at the trailing edges. The current-sheet thicknesses at both the leading and trailing edges are estimated to be on the ion-inertial scale, and thinner current at the trailing edges is consistent with the fact that MMS detect more reconnection jets there. Furthermore, our findings are in agreement with the results in Ma et al. (2014a), who illustrated that the initiation of K-H waves induces deformation within the current layer. Stronger thinning effect at the trailing edges results in higher current densities and higher observational probability of reconnection signature. Besides, the 31st current sheet is different from other current sheets, with a northward jet and parallel-moving energetic electrons (as shown in Figure S1 of the Supporting Information S1). It may result from the secondary reconnection (Huang et al., 2015; Lapenta et al., 2015; Tang et al., 2021).

In this event, the current sheets of both the leading and trailing edges can be compressed down to ion scale, satisfying the triggering condition of magnetic reconnection (Figure 4c). Stronger compression effect at the trailing edges lead to more frequent observations of the reconnection jets. After the reconnection was triggered at the K-H boundary during southward IMF, the expansion of the reconnection outflow could broaden the magnetosphere-magnetosheath boundary layer, which may weaken the generation and evolution of the K-H waves. The velocity shear between the magnetospheric ($+B_L$) and magnetosheath ($-B_L$) sections of the reconnected field lines may generate a significant in-plane component (B_M and B_N). This could also restrain the K-H evolution. As a comparison, the magnetic shear angle is initially small at the low-latitude magnetopause during northward IMF. Nonlinear evolution of the K-H waves can distort the magnetic field lines across the magnetopause and increase the local magnetic shear. This process may create an intense current sheet along the trailing edge where the magnetosheath flow generates strong compression. Consequently, magnetic reconnection is primarily initiated at the trailing edge, with the X-line typically aligning with the direction of the K-H vortex axis, as shown in Figure 4d (Eriksson et al., 2016; Li et al., 2016; Nakamura et al., 2006). In such a scenario, the X-line could be significantly shorter compared to that formed during southward IMF, and reconnection takes place within a highly localized region. Therefore, the evolution of K-H waves during northward IMF may not be significantly suppressed by the induced magnetic reconnection process.

The widespread occurrence of magnetic reconnection during southward IMF may impact the evolution of K-H waves through (a) boundary-layer broadening due to the latitudinal expansion of the reconnection exhaust and (b) complex flow and magnetic field patterns in the broadened boundary layer. The presence of widely distributed X-line along the K-H wave surface could have a substantial suppressive effect on the K-H waves, which may be responsible for the low observational probability of K-H waves under southward IMF.

Data Availability Statement

The OMNI data were provided via https://spdf.gsfc.nasa.gov/pub/data/omni/. MMS observations are publicly available via NASA resources and the MMS Science Data Center at CU/LASP (https://lasp.colorado.edu/mms/sdc/public/about/browse-wrapper/). The MMS data are analyzed using the IRFU-Matlab package (https://github.com/irfu/irfu-matlab). All MMS data utilized in this study is sourced from MMS L2 Data Products. For FPI (Fast Plasma Investigation) and FGM (Fluxgate Magnetometer), the CDF-file versions used are 3.3.0 and 5.251.0, respectively. Regarding EDP (Electric Double Probes), the CDF-file versions for the burst- and fast-modes are 3.0.2 and 3.0.1, respectively.

References

Balogh, A., & Treumann, R. A. (2013). Quasi-perpendicular supercritical shocks. In A. Balogh, & R. A. Treumann (Eds.), *Physics of collisionless shocks: Space plasma shock waves* (pp. 149–220). Springer. https://doi.org/10.1007/978-1-4614-6099-2_5

Blasl, K. A., Nakamura, T. K. M., Plaschke, F., Nakamura, R., Hasegawa, H., Stawarz, J. E., et al. (2022). Multi-scale observations of the magnetopause Kelvin–Helmholtz waves during southward IMF. *Physics of Plasmas*, *29*(1), 012105. https://doi.org/10.1063/5.0067370

Cassak, P. A., & Shay, M. A. (2007). Scaling of asymmetric magnetic reconnection: General theory and collisional simulations. *Physics of Plasmas*, *14*(10), 102114. https://doi.org/10.1063/1.2795630

Chandrasekhar, S. (1961). *Hydrodynamic and hydromagnetic stability*. Oxford University Press.

Claudepierre, S. G., Elkington, S. R., & Wiltberger, M. (2008). Solar wind driving of magnetospheric ULF waves: Pulsations driven by velocity shear at the magnetopause. *Journal of Geophysical Research*, *113*(A5), A05218. https://doi.org/10.1029/2007JA012890

Ergun, R. E., Tucker, S., Westfall, J., Goodrich, K. A., Malaspina, D. M., Summers, D., et al. (2016). The axial double probe and fields signal processing for the MMS mission. *Space Science Reviews*, *199*(1), 167–188. https://doi.org/10.1007/s11214-014-0115-x

Eriksson, S., Wilder, R., Ergun, R. E., Schwartz, S. J., Cassak, P., Burch, J. L., et al. (2016). Magnetospheric multiscale observations of the electron diffusion region of large guide field magnetic reconnection. *Physical Review Letters*, *117*(1), 015001. https://doi.org/10.1103/PhysRevLett.117.015001

Fairfield, D. H. (1971). Average and unusual locations of the Earth's magnetopause and bow shock. *Journal of Geophysical Research*, *76*(28), 6700–6716. https://doi.org/10.1029/JA076i028p06700

Fairfield, D. H., Otto, A., Mukai, T., Kokubun, S., Lepping, R. P., Steinberg, J. T., et al. (2000). Geotail observations of the Kelvin-Helmholtz instability at the equatorial magnetotail boundary for parallel northward fields. *Journal of Geophysical Research*, *105*(A9), 21159–21173. https://doi.org/10.1029/1999JA000316

Guo, X. C., Wang, C., & Hu, Y. Q. (2010). Global MHD simulation of the Kelvin-Helmholtz instability at the magnetopause for northward interplanetary magnetic field. *Journal of Geophysical Research*, *115*(A10), A10218. https://doi.org/10.1029/2009JA015193

Haaland, S., Paschmann, G., Øieroset, M., Phan, T., Hasegawa, H., Fuselier, S. A., et al. (2020). Characteristics of the flank magnetopause: MMS results. *Journal of Geophysical Research: Space Physics*, *125*(3), e2019JA027623. https://doi.org/10.1029/2019JA027623

Hasegawa, H., Fujimoto, M., Phan, T.-D., Rème, H., Balogh, A., Dunlop, M. W., et al. (2004). Transport of solar wind into Earth's magnetosphere through rolled-up Kelvin–Helmholtz vortices. *Nature*, *430*(7001), 755–758. https://doi.org/10.1038/nature02799

Hasegawa, H., Fujimoto, M., Takagi, K., Saito, Y., Mukai, T., & Rème, H. (2006). Single-spacecraft detection of rolled-up Kelvin-Helmholtz vortices at the flank magnetopause. *Journal of Geophysical Research*, *111*(A9), A09203. https://doi.org/10.1029/2006JA011728

Hasegawa, H., Retinò, A., Vaivads, A., Khotyaintsev, Y., André, M., Nakamura, T. K. M., et al. (2009). Kelvin-Helmholtz waves at the Earth's magnetopause: Multiscale development and associated reconnection. *Journal of Geophysical Research*, *114*(A12), A12207. https://doi.org/10.1029/2009JA014042

Huang, C., Lu, Q., Guo, F., Wu, M., Du, A., & Wang, S. (2015). Magnetic islands formed due to the Kelvin-Helmholtz instability in the outflow region of collisionless magnetic reconnection. *Geophysical Research Letters*, *42*(18), 7282–7286. https://doi.org/10.1002/2015GL065690

Hwang, K.-J., Kuznetsova, M. M., Sahraoui, F., Goldstein, M. L., Lee, E., & Parks, G. K. (2011). Kelvin-Helmholtz waves under southward interplanetary magnetic field. *Journal of Geophysical Research*, *116*(A8), A08210. https://doi.org/10.1029/2011JA016596

Kronberg, E. A., Gorman, J., Nykyri, K., Smirnov, A. G., Gjerloev, J. W., Grigorenko, E. E., et al. (2021). Kelvin-Helmholtz instability associated with reconnection and ultra low frequency waves at the ground: A case study. *Frontiers in Physiology*, *9*. https://doi.org/10.3389/fphy.2021.738988

Lapenta, G., Markidis, S., Goldman, M. V., & Newman, D. L. (2015). Secondary reconnection sites in reconnection-generated flux ropes and reconnection fronts. *Nature Physics*, *11*(8), 690–695. https://doi.org/10.1038/nphys3406

Li, W. Y., André, M., Khotyaintsev, Y. V., Vaivads, A., Graham, D. B., Toledo-Redondo, S., et al. (2016). Kinetic evidence of magnetic reconnection due to Kelvin-Helmholtz waves. *Geophysical Research Letters*, *43*(11), 5635–5643. https://doi.org/10.1002/2016GL069192

Li, W. Y., Guo, X. C., & Wang, C. (2012). Spatial distribution of Kelvin-Helmholtz instability at low-latitude boundary layer under different solar wind speed conditions. *Journal of Geophysical Research*, *117*(A8), A08230. https://doi.org/10.1029/2012JA017780

Li, W. Y., Wang, C., Tang, B., Guo, X., & Lin, D. (2013). Global features of Kelvin-Helmholtz waves at the magnetopause for northward interplanetary magnetic field. *Journal of Geophysical Research: Space Physics*, *118*(8), 5118–5126. https://doi.org/10.1002/jgra.50498

Lin, D., Wang, C., Li, W., Tang, B., Guo, X., & Peng, Z. (2014). Properties of Kelvin-Helmholtz waves at the magnetopause under northward interplanetary magnetic field: Statistical study. *Journal of Geophysical Research: Space Physics*, *119*(9), 7485–7494. https://doi.org/10.1002/2014JA020379

Lindqvist, P.-A., Olsson, G., Torbert, R. B., King, B., Granoff, M., Rau, D., et al. (2016). The spin-plane double probe electric field instrument for MMS. *Space Science Reviews*, *199*(1), 137–165. https://doi.org/10.1007/s11214-014-0116-9

Lu, S. W., Wang, C., Li, W. Y., Tang, B. B., Torbert, R. B., Giles, B. L., et al. (2019). Prolonged Kelvin–Helmholtz waves at dawn and dusk flank magnetopause: Simultaneous observations by MMS and THEMIS. *The Astrophysical Journal*, *875*(1), 57. https://doi.org/10.3847/1538-4357/ab0e76

Ma, X., Otto, A., & Delamere, P. A. (2014a). Interaction of magnetic reconnection and Kelvin-Helmholtz modes for large magnetic shear: 1. Kelvin-Helmholtz trigger. *Journal of Geophysical Research: Space Physics*, *119*(2), 781–797. https://doi.org/10.1002/2013JA019224

Ma, X., Otto, A., & Delamere, P. A. (2014b). Interaction of magnetic reconnection and Kelvin-Helmholtz modes for large magnetic shear: 2. Reconnection trigger: Ma et al. *Journal of Geophysical Research: Space Physics*, *119*(2), 808–820. https://doi.org/10.1002/2013JA019225

Miura, A., & Pritchett, P. L. (1982). Nonlocal stability analysis of the MHD Kelvin-Helmholtz instability in a compressible plasma. *Journal of Geophysical Research*, *87*(A9), 7431–7444. https://doi.org/10.1029/JA087iA09p07431

Nakamura, T. K. M., Blasl, K. A., Hasegawa, H., Umeda, T., Liu, Y.-H., Peery, S. A., et al. (2022). Multi-scale evolution of Kelvin–Helmholtz waves at the Earth's magnetopause during southward IMF periods. *Physics of Plasmas*, *29*(1), 012901. https://doi.org/10.1063/5.0067391

Nakamura, T. K. M., Daughton, W., Karimabadi, H., & Eriksson, S. (2013). Three-dimensional dynamics of vortex-induced reconnection and comparison with THEMIS observations. *Journal of Geophysical Research: Space Physics*, *118*(9), 5742–5757. https://doi.org/10.1002/jgra.50547

Nakamura, T. K. M., Eriksson, S., Hasegawa, H., Zenitani, S., Li, W. Y., Genestreti, K. J., et al. (2017). Mass and energy transfer across the Earth's magnetopause caused by vortex-induced reconnection. *Journal of Geophysical Research: Space Physics*, *122*(11), 11505–11522. https://doi.org/10.1002/2017JA024346

Nakamura, T. K. M., Fujimoto, M., & Otto, A. (2006). Magnetic reconnection induced by weak Kelvin-Helmholtz instability and the formation of the low-latitude boundary layer. *Geophysical Research Letters*, *33*(14), L14106. https://doi.org/10.1029/2006GL026318

Nakamura, T. K. M., Hayashi, D., Fujimoto, M., & Shinohara, I. (2004). Decay of MHD-scale Kelvin-Helmholtz vortices mediated by parasitic electron dynamics. *Physical Review Letters*, *92*(14), 145001. https://doi.org/10.1103/PhysRevLett.92.145001

Nakamura, T. K. M., Plaschke, F., Hasegawa, H., Liu, Y.-H., Hwang, K.-J., Blasl, K. A., & Nakamura, R. (2020). Decay of Kelvin-Helmholtz vortices at the Earth's magnetopause under pure southward IMF conditions. *Geophysical Research Letters*, *47*(13), e2020GL087574. https://doi.org/10.1029/2020GL087574

Nykyri, K., Ma, X., Dimmock, A., Foullon, C., Otto, A., & Osmane, A. (2017). Influence of velocity fluctuations on the Kelvin-Helmholtz instability and its associated mass transport. *Journal of Geophysical Research: Space Physics*, *122*(9), 9489–9512. https://doi.org/10.1002/2017JA024374

Nykyri, K., & Otto, A. (2001). Plasma transport at the magnetospheric boundary due to reconnection in Kelvin-Helmholtz vortices. *Geophysical Research Letters*, *28*(18), 3565–3568. https://doi.org/10.1029/2001GL013239

Nykyri, K., Otto, A., Lavraud, B., Mouikis, C., Kistler, L. M., Balogh, A., & Rème, H. (2006). Cluster observations of reconnection due to the Kelvin-Helmholtz instability at the dawnside magnetospheric flank. *Annales Geophysicae*, *24*(10), 2619–2643. https://doi.org/10.5194/angeo-24-2619-2006

Paschmann, G., & Daly, P. W. (1998). *Analysis methods for multi-spacecraft data*. ISSI scientific reports series SR-001, ESA/ISSI (Vol. 1). ISSI Scientific Reports Series, 1. ISBN 1608-280X.

Phan, T. D., Dunlop, M. W., Paschmann, G., Klecker, B., Bosqued, J. M., Rème, H., et al. (2004). Cluster observations of continuous reconnection at the magnetopause under steady interplanetary magnetic field conditions. *Annales Geophysicae*, *22*(7), 2355–2367. https://doi.org/10.5194/angeo-22-2355-2004

Plaschke, F., Kahr, N., Fischer, D., Nakamura, R., Baumjohann, W., Magnes, W., et al. (2016). Steepening of waves at the duskside magnetopause. *Geophysical Research Letters*, *8*(14), 7373–7380. https://doi.org/10.1002/2016GL070003

Pollock, C., Moore, T., Jacques, A., Burch, J., Gliese, U., Saito, Y., et al. (2016). Fast plasma investigation for magnetospheric multiscale. *Space Science Reviews*, *199*(1), 331–406. https://doi.org/10.1007/s11214-016-0245-4

Pu, Z.-Y., & Kivelson, M. G. (1983a). Kelvin-Helmholtz Instability at the magnetopause: Energy flux into the magnetosphere. *Journal of Geophysical Research*, *88*(A2), 853–861. https://doi.org/10.1029/JA088iA02p00853

Pu, Z.-Y., & Kivelson, M. G. (1983b). Kelvin:Helmholtz instability at the magnetopause: Solution for compressible plasmas. *Journal of Geophysical Research*, *88*(A2), 841–852. https://doi.org/10.1029/JA088iA02p00841

Russell, C. T., Anderson, B. J., Baumjohann, W., Bromund, K. R., Dearborn, D., Fischer, D., et al. (2016). The magnetospheric multiscale magnetometers. *Space Science Reviews*, *199*(1), 189–256. https://doi.org/10.1007/s11214-014-0057-3

Sckopke, N., Paschmann, G., Haerendel, G., Sonnerup, B. U. Ö., Bame, S. J., Forbes, T. G., et al. (1981). Structure of the low-latitude boundary layer. *Journal of Geophysical Research*, *86*(A4), 2099–2110. https://doi.org/10.1029/JA086iA04p02099

Settino, A., Khotyaintsev, Y. V., Graham, D. B., Perrone, D., & Valentini, F. (2022). Characterizing satellite path through Kelvin-Helmholtz instability using a mixing parameter. *Journal of Geophysical Research: Space Physics*, *127*(2), e2021JA029758. https://doi.org/10.1029/2021JA029758

Settino, A., Perrone, D., Khotyaintsev, Y. V., Graham, D. B., Valentini, F., & Perrone, D. (2021). Kinetic features for the identification of Kelvin–Helmholtz vortices in in situ observations. *The Astrophysical Journal*, *912*(2), 154. https://doi.org/10.3847/1538-4357/abf1f5

Shue, J.-H., Song, P., Russell, C. T., Steinberg, J. T., Chao, J. K., Zastenker, G., et al. (1998). Magnetopause location under extreme solar wind conditions. *Journal of Geophysical Research*, *103*(A8), 17691–17700. https://doi.org/10.1029/98JA01103

Sonnerup, B. U. Ö. (1980). Theory of the low-latitude boundary layer. *Journal of Geophysical Research*, *85*(A5), 2017–2026. https://doi.org/10.1029/JA085iA05p02017

Stawarz, J. E., Eriksson, S., Wilder, F. D., Ergun, R. E., Schwartz, S. J., Pouquet, A., et al. (2016). Observations of turbulence in a Kelvin-Helmholtz event on 8 September 2015 by the magnetospheric multiscale mission. *Journal of Geophysical Research: Space Physics*, *121*(11), 11021–11034. https://doi.org/10.1002/2016JA023458

Takagi, K., Hashimoto, C., Hasegawa, H., Fujimoto, M., & TanDokoro, R. (2006). Kelvin-Helmholtz instability in a magnetotail flank-like geometry: Three-dimensional MHD simulations. *Journal of Geophysical Research*, *111*(A8), A08202. https://doi.org/10.1029/2006JA011631

Tang, B. B., Li, W. Y., Wang, C., Khotyaintsev, Y. V., Graham, D. B., Zhang, Q. H., et al. (2021). Secondary magnetic reconnection at Earth's flank magnetopause. *Frontiers in Astronomy and Space Sciences*, *8*. https://doi.org/10.3389/fspas.2021.740560

Taylor, M. G. G. T., Hasegawa, H., Lavraud, B., Phan, T., Escoubet, C. P., Dunlop, M. W., et al. (2012). Spatial distribution of rolled up Kelvin-Helmholtz vortices at Earth's dayside and flank magnetopause. *Annales Geophysicae*, *30*(6), 1025–1035. https://doi.org/10.5194/angeo-30-1025-2012

Vedenov, A., & Sagdeev, R. (1961). Some properties of a plasma with an anisotropic ion velocity distribution in a magnetic field (Vol. *1*, p. 332).

Vernisse, Y., Lavraud, B., Eriksson, S., Gershman, D. J., Dorelli, J., Pollock, C., et al. (2016). Signatures of complex magnetic topologies from multiple reconnection sites induced by Kelvin-Helmholtz instability. *Journal of Geophysical Research: Space Physics*, *121*(10), 9926–9939. https://doi.org/10.1002/2016JA023051

Vernisse, Y., Lavraud, B., Faganello, M., Fadanelli, S., Sisti, M., Califano, F., et al. (2020). Latitudinal dependence of the Kelvin-Helmholtz instability and beta dependence of vortex-induced high-guide field magnetic reconnection. *Journal of Geophysical Research: Space Physics*, *125*(5), e2019JA027333. https://doi.org/10.1029/2019JA027333

Wang, J.-Q., Yang, Y., Khan, S., Wang, X.-L., Yuan, H.-X.-Y., & Duan, W.-S. (2023). Jets with Kelvin-Helmholtz waves at the Earth's magnetopause under pure southward IMF conditions. *Astrophysics and Space Science*, *368*(3), 12. https://doi.org/10.1007/s10509-023-04168-4

Yan, G. Q., Mozer, F. S., Shen, C., Chen, T., Parks, G. K., Cai, C. L., & McFadden, J. P. (2014). Kelvin-Helmholtz vortices observed by THEMIS at the duskside of the magnetopause under southward interplanetary magnetic field. *Geophysical Research Letters*, *41*(13), 4427–4434. https://doi.org/10.1002/2014GL060589